Invited Paper

Near-field scanning optical microscopy imaging: theory, simulation and experiment

Garnett W. Bryant and Ansheng Liu

National Institute of Standards and Technology, Gaithersburg, MD 20899-8423,USA

ABSTRACT

Near-field scanning optical microscopy (NSOM) is being studied to achieve optical resolution much better than the diffraction limit. Improved resolution is realized when the sample is in the near field of the probe. Strong near-field coupling between sample and probe complicates image analysis. Experiments with well characterized tips and simple samples are needed to produce basic NSOM images. Detailed modeling able to reproduce images and identify essential features in image formation is required. We analyze experimental NSOM transmission images of nanochannel glass arrays and of Au nanoparticles obtained in illumination mode. We use several approaches, including the discrete dipole method and the transfer matrix method, to simulate these images. Experimental and simulated images are compared to identify the contributions of tip-field structure, sample scattering, and the collection process to the images and to provide a clearer interpretation of these NSOM images.

Keywords: near-field optics, optical microscopy, imaging, simulation

1. INTRODUCTION

Near-field scanning optical microscopy (NSOM) is an exciting new class of optical microscopies which can provide optical resolution much better than the diffraction limit.[1–4] In illumination-mode NSOM an aperture that is much smaller than the wavelength, λ, of the light is used as a nearly point-like (on the scale of λ) light source. Typically, an optical fiber is pulled to a 20-100 nm tip and metal coated, leaving a small hole in the metal coating at the end of the tip to provide a nanometer-scale aperture. This aperture is placed very close to the sample surface so that light emitted from the aperture does not diffract significantly before reaching the sample and superresolution, well below the diffraction limit $\lambda/2$, can be achieved. Components of the light that are strongly localized laterally by the aperture are evanescent, decaying rapidly as they move away from the aperture. Tip/sample distance can be adjusted to control the contribution from these evanescent tip fields. In a similar manner, in collection mode an aperture probe is used to collect the near field scattered by a sample. In fact, the same aperture probe can be used in both illumination and collection mode. NSOM images can also be obtained with an apertureless probe. In this case, a sharp metallic or dielectric tip is used to scatter sample near-fields to the far field where they are collected to image the sample.

NSOM images can now be readily obtained. A key step to the further development and application of NSOM is learning how to interpret, understand, and analyze these images. In NSOM, the excitation, the detection, or both occur in the near field. Strong coupling between the sample and the light source/detector, which is not present in far-field optical microscopy, will occur in NSOM. In transmission (reflection) NSOM, light from the metallized fiber tip couples to the sample in the near field of the tip, while the light transmitted (reflected) from the sample is collected in the far field. The NSOM images are influenced both by the strong sample/source coupling and by the far-field optics of the collection process. To understand these images one must know how structure in the tip field influences the images, how the localized source field is influenced by the presence of the sample in the near field, how light scatters from the sample, how interference between tip and scattered fields modulates the images, and how light is collected in the far field. To fully exploit the potential of NSOM, one must interpret images generated when the separation between the strongly coupled tip and sample is varied and be able to separate effects due to the structure in the tip fields, the sample scattering, the mutual interaction, and the interference effects.

To obtain a clearer understanding of image formation in NSOM, careful experiments with well characterized tips and simple samples are needed to produce the basic images expected in NSOM. To complement experiments, a detailed theory capable of reproducing the images and identifying the essential features in the image formation

Send correspondence to G.W.B.; E-mail: garnett.bryant@nist.gov

Part of the SPIE Conference on Optical Pulse and Beam Propagation • San Jose, California
January 1999 SPIE Vol. 3609 • 0277-786X/99/$10.00

is needed. It is important that the theory model the entire process of image formation, including the illumination, scattering and collections processes on equal footing, so that all contributions to the image formation can be identified. In this paper we discuss illumination-mode NSOM transmission images that were made of nanochannel glass (NCG) arrays and of Au nanoparticles. In each case, the samples are simple with well characterized geometry and dielectric profile. We discuss calculations performed to simulate these images based on theories that model the entire process, including the illumination, scattering, and collection. Experimental and simulated images are compared to identify the essential features of image formation for these two cases, such as the importance of local field effects, the sensitivity to tip fields and tip parameters, and which field components control the image formation. We use the results to characterize the contributions of illumination, scattering, and collection to the image formation.

2. IMAGING NANOCHANNEL GLASS ARRAYS

We first consider transmission NSOM images[5] made recently of a nanochannel-glass (NCG) array.[6] These images probe the optical mode structure of this two-dimensional (2D) photonic crystal.[7] The NCG array studied is a 2D triangular array of glass rods in a matrix made from a lower-index glass. By heating and pulling this structure the lattice constants of the array can be controlled. High quality NCGs with lattice spacings on the order of or much less than λ can be made. The geometry is well characterized by scanning force microscopy. The surfaces that are scanned have nearly flat topography. For these reasons, NCGs provide excellent samples for testing NSOM.

The index variation of the NCG array is periodic in the 2D plane perpendicular to the glass rods, so the array possesses the optical modes of a 2D photonic crystal. Because the glass rods have the higher index, the distribution of these photonic modes in this 2D plane tends to be larger in the glass rods. However the index mismatch between core and matrix glasses is small for the sample studied, so significant coupling of these photonic modes among neighboring cores occurs as well. A comparison between theory and experiment will show what information about the 2D spatial distribution of the NCG photonic crystal modes can be learned from probing with transmission NSOM.

2.1. Experimental results

The transmission NSOM experiment is shown schematically in Fig. 1. A metal-coated fiber NSOM tip was placed about 10 nm from the sample surface. Light transmitted through the sample was collected in the far field by an objective with numerical aperture NA. In free space the numerical aperture $NA = \sin(\theta)$ where θ is the half angle of the acceptance cone. The NCG array was scanned in x and y at constant separation above the tip to produce a 2D image. The images were taken with two different wavelengths of light ($\lambda = 670$ nm and $\lambda = 488$ nm). Polarization of the light leaving the fiber tip was controlled by use of fiber paddles. Light was collected for three different NA ($NA = 0.28, 0.55, 0.7$). In the NCG array, the channel glass was cylindrical, approximately 745 nm in diameter with center-to-center nearest neighbor separation of 1.07 ± 0.05 μm. The index of refraction of the matrix glass was 1.65-1.68 and that of the channel glass was 0.2% to 1.2% higher in the visible range.

The detailed results for this experiment, including the gray-scale images made by transmission NSOM and line scans from these gray-scale images, are presented in Ref. 5. We summarize here the key findings. For low NA of the collection optics ($NA = 0.28$), the gray-scale images exhibit a triangular array of bright, circular spots with approximately 55% optical contrast between the bright regions, with maximum intensity I_b, and the dark regions, with minimum intensity I_d. The optical contrast is the change in intensity normalized by the average intensity $2(I_b - I_d)/(I_b + I_d)$. The center of a spot corresponds to the tip below the center of a channel-glass core. Similar results are seen for both λ. For intermediate NA ($NA = 0.55$), the images for the two λ are different. For the longer wavelength ($\lambda = 670$ nm), the bright spots flatten, the light to dark contrast is reduced to 38%, and the overall signal level increases. For the shorter wavelength ($\lambda = 488$ nm), the bright spots becomes rings, brightest when the tip is near but not at the channel glass edge, weaker when near the center of the channel glass core, and weakest outside the channel glass. The light to dark contrast is reduced to 25%. At the highest NA ($NA = 0.70$) this ring structure persists for the shorter wavelength with the contrast reduced to 15%. For the longer wavelength this ring structure begins to appear and the the contrast ratio is reduced to 28%. These results are independent of the polarization of the tip field and weakly dependent on the aperture size and the tip/sample separation in the near field. Typical line scans are shown in Fig. 2 for $NA = 0.70$ with the tip about 10 nm from the sample. The scans were done along x, the direction between two adjacent glass cores, as shown in Fig. 1.

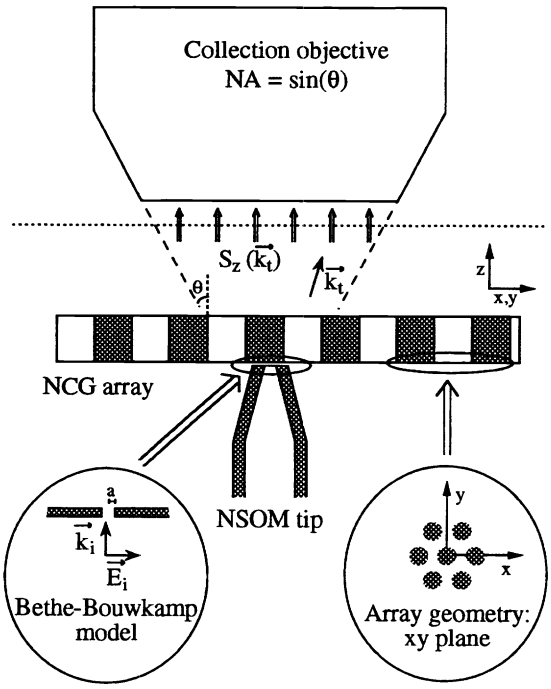

Figure 1. Schematic of the transmission NSOM experiment. The nanochannel-glass array sample is scanned at constant separation across the NSOM tip. The transmitted light is collected by an objective with numerical aperture NA. Key elements of the theory are represented schematically. The tip field is described by the Bethe-Bouwkamp model[9–11]. The collected light is modeled as the total flux that leaves the sample inside the acceptance cone defined by NA and passes through a plane, as indicated, in the far field. The array geometry is indicated.

2.2. Theory

A complete theory for NSOM imaging of NCGs requires a model for the tip field, a calculation of the optical modes of the NCG, a calculation for the transmission of the illuminating tip field through the NCG, a model for the collection by a lens in the far-field, and a model for the NCG. This theory is outlined in Fig. 1. The details are given in Ref. 8. The key elements are summarized here.

Rigorous, three-dimensional calculations of the fields emitted by a tip with a nanometer aperture are difficult and numerically intensive. The Bethe-Bouwkamp (BB) model[9–11] is a simple approach that is commonly used instead of the numerically intensive approaches to model the tip field. To simulate NSOM images of NCGs we use the BB model. As our results show, the BB model provides an adequate representation for the tip-fields in these experiments. In the Bethe-Bouwkamp model, the tip near field is modeled by the near field of the light transmitted by a circular aperture with radius a, in a perfectly conducting, thin, metal screen when a linearly polarized, plane-wave field is incident normal to the screen (see Fig. 1).

When the modes of a 2D photonic crystal are determined, the band structure for the mode frequency, ω versus k_x and k_y, is found typically for $k_z = 0$.[7] To model transmission through an NCG, we need a different set of the optical modes; we need all propagating and evanescent modes, all k_z, for a given k_x, k_y, and ω. For that reason, we solve an eigenvalue problem for k_z rather than an eigenvalue problem for ω. We begin from the Maxwell equations for electric and magnetic fields, $\mathbf{E}$ and $\mathbf{B}$, with frequency ω. We expand the fields in terms of the Fourier components in 2D reciprocal lattice space, write the Maxwell equations in reciprocal space and solve the resulting eigenvalue equation for k_z to find the allowed optical modes.

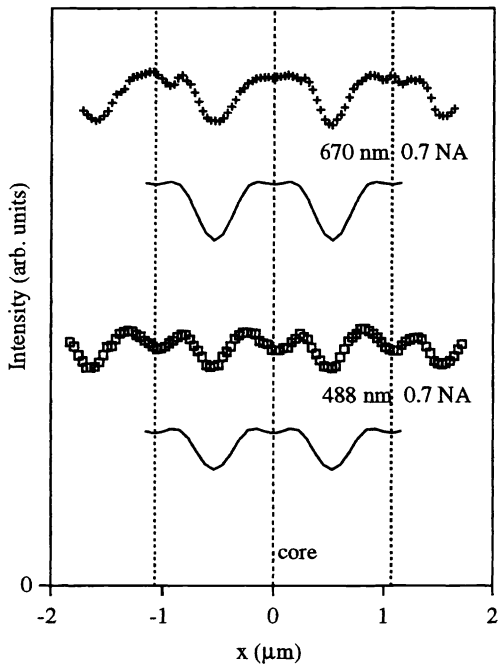

Figure 2. Transmission as the tip scans along x: experimental scans (□,+) and calculated scans (——) scaled to have the same average intensity and shifted for clarity. The core-glass centers are marked by vertical dashed lines. At $x = 0$ the tip and core glass centers are aligned.

We determine the transmission of the incident tip field through the NCG by solving the standard boundary matching problem for transmission through a film. We assume that the total field in the free-space region containing the tip is the incident tip field plus the field reflected by the NCG. Reflections off the tip are not included. This is the only approximation, other than the use of the Bethe-Bouwkamp model for the source field, that we make for the local fields near the tip. At each NCG surface, we have the boundary conditions that the tangential electric field and the tangential magnetic field be continuous. These conditions define the matrix equations that are solved to determine the amplitudes for the reflected and transmitted fields and for the excited NCG modes. To model transmission-NSOM images, we calculate the transmitted light that is collected by optics with a numerical aperture NA. We assume that the optics collects all of the transmitted flux that passes through an x-y plane in the far-field away from the NCG. All flux leaving the NCG within the numerical aperture of the optics, the angle θ in Fig. 1, is collected.

As shown in Fig. 1, the NCG sample is a 2D triangular lattice of glass rods in a glass matrix. We assume that rods are perfect cylinders. In the experiments, the lattice spacing is 1.07 μm and the core radius is 0.37 μm. The measured samples are approximately 250 μm thick. We use this thickness to model the measured images. Our results for thick samples are insensitive to sample thickness because we eliminate Fabry-Perot oscillations by use of a damping factor to break the coherence of multiple reflections between the NCG surfaces. We assume that the index of refraction is real and uniform in each glass, has the bulk value in each glass,[5] and has a step discontinuity at the core/matrix glass interface. This is the only assumption that we make about the dielectric structure of the NCG.

2.3. Simulations

First, we show that the theory is able to describe the images of the NCG made with transmission NSOM. Calculated line scans along x of the transmitted intensity are shown in Fig. 3 for $\lambda = 488$ nm. Similar results are obtained for $\lambda = 670$ nm. The dependence on NA is shown. The calculated line scans reproduce the key features in the measured line scans. For small NA, the line scans are peaked at the channel glass centers, with a peak/valley intensity ratio of about 1.5, even though the index contrast is only 1-2%. As NA increases, more of the transmitted light is collected

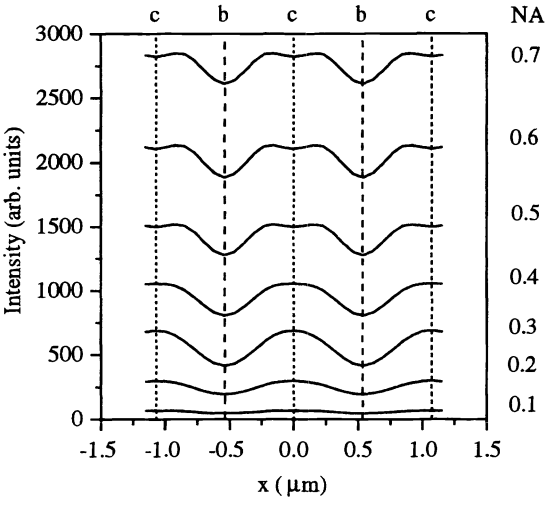

Figure 3. Transmitted intensity line scan along x: $\lambda = 488$ nm, tip/sample separation $z_{ap} = 10$ nm, tip radius $a = 50$ nm. Dependence on collection optics NA is shown. Positions of channel-glass centers (c) and bridge sites (b), the midpoints on the lines joining adjacent glass centers, are shown.

and the average transmitted intensity increases. The peaks broaden and flatten and the peak/valley ratio decreases. At $NA = 0.5$ for $\lambda = 488$ nm, the peaks about core centers develop structure with depressions in the middle and side peaks ≈ 0.2 μm from the centers. These side peaks produce the ring structure observed in the experimental images. The experimental images at 0.7 NA show the rings prominently for $\lambda = 488$ nm but only hint that rings are starting to appear for $\lambda = 670$ nm. Our calculations show that the rings form at lower NA for shorter λ. This occurs because more of the photonic mode k-space is collected, for a given NA, for shorter λ. Scans along other directions give similar results. In particular, the structure inside the glass core is identical for the scans along different directions, confirming the cylindrical symmetry of this structure. This gives evidence that the structure in the peak is due to transmitted light that propagates through the sample in photonic modes that are concentrated in the cylindrically symmetric cores.

Figure 2 shows a comparison of the experimental and calculated line scans along x at $NA = 0.7$ for both λ. The curves have been scaled to have the same average value and then shifted for clarity. There is strong qualitative agreement between the data and the calculations, as we have already discussed. The ring structure occurs at similar positions, well inside the edge of the channel glass, in both the experimental and calculated scans. This ring structure is not directly related to the channel glass edge but is connected to the spatial distribution of NCG photonic modes. At low NA, the lowest photonic mode makes the dominant contribution to the images, so the peak image intensity is at core centers. At higher NA, higher photonic modes contribute and produce the ring structure in the images. The calculated line scans depend only weakly on the polarization of the tip field, the tip/sample separation, and the aperture size, just as in the experimental images.

From our comparison of experimental and simulated images, we find that these images provide information about the spatial distribution of the photonic modes of the sample rather than directly about the geometry of the dielectric profile. The images depend sensitively on the collection optics because the NA determines which modes can be collected in transmission. These images are insensitive to the details of the tip field (and the simple BB model is adequate) because the spatial distribution of the dominant photonic modes in the channel glass is much broader than the spread of the tip field.

3. IMAGING AU NANOPARTICLES

The NSOM images of NCG arrays provide information about the sample fields and are insensitive to the detailed structure of the tip field. We now present an example where the NSOM images depend critically on the tip field and

the images provide information about both the tip fields and the sample. We show from a comparison of experimental and simulated images[12,13] that the images can only be understood with a model that correctly accounts for the geometry of the tip and accurately reproduces the tip fields. Simple models, such as the Bethe-Bouwkamp model, are not able the reproduce the experimental images.

We consider transmission NSOM images[12] made recently of 100 nm Au nanoparticles in illumination mode. The particles are simple with topography well defined by scanning force microscopy. The images were taken at wavelengths well away from any particle resonance. Thus, simple images are expected. As our results show, the images are complicated by the structure in the tip fields and a careful analysis is needed is to separate the contributions of the tip field, the sample scattering, and interference effects to the image formation.

3.1. Experimental results

The transmission NSOM experiment is the same as that shown in Fig. 1 except that the sample is an individual Au nanoparticle on a silanized glass surface rather than the NCG array. The NSOM microscope used is a beetle-style scanner assembly located inside an ellipsoidal cavity with an Al-coated NSOM tip at one cavity foci.[14] The cavity allows efficient, symmetric collection of reflected light, simultaneous with transmission. In this study all images were recorded in transmission after illumination with 488 nm light from the tip. Use of $\lambda/4$ and $\lambda/2$ wave-plates allowed control of the illumination polarization state. Probe fly-height control was achieved by shear-force damping of the tip. Care must be taken in the interpretation of NSOM images to avoid artifacts due to topographic feedthrough. A scanning mode was utilized in which tip retraction curves (z-scans) were recorded for each point in a 2D (xy) scan of the sample after establishing shear-force engagement. The resultant 4D data structures (xyz and optical signal) allowed reconstruction of both constant-gap and constant-height optical images. The samples were Au nanoparticles, approximately 100 nm in diameter. Two types of Al-coated tips were used. Blunt tips with an Al-coating thickness greater than $\lambda/2$ were used. Sharper tips with thinner cladding were also used. In each case, the aperture diameter was about 140 nm. These two types of tips produced very different images.

Topographic scans of the particles made with the NSOM tip indicate that the particles are 60 nm high, consistent with the expected particle diameter. The base-widths of the topographic features made with blunt tips are greater than 800 nm. This indicates that the tip diameter is greater than 700 nm and the cladding thickness is greater than 250 nm. Transmission images correlate with the geometry of the tip. Blunt tips with a thick Al cladding show a distinctive triplet structure for scans along one direction (here labeled x) with a broad central minimum when the tip and Au particle are centered and side maxima when the cladding is above the particle. The separation between the two maxima is about 280 nm, the central minimum has a FWHM of about 140 nm. For y-scans, the central minimum is significantly broader (about 280 nm FWHM) and there are no side maxima. Sharp tips with a much thinner cladding show a central symmetric minimum (FWHM is about 280 nm) but no side maxima. For sharp tips, interference oscillations occur when the tip and particle are widely separated in a y-scan. No interference oscillations are seen in x-scans. When the input polarization of the tip field is rotated by 90° the images rotate by 90° .

3.2. Theory

To understand the experimental findings, we performed numerical calculations of the light power collected when scanning the NSOM tip over the Au particle along the directions parallel and perpendicular to the polarization direction of the incident field that drives the fiber tip.[12,13] The tip scans close to the sample, so the tip end most strongly interacts with the particle and should make the dominant contribution to the image formation. To simplify our calculations, we only model the contribution from the tip end. We model the end of the metal-coated tip as a thin disk. The interior (core) part of the disk is glass and serves as an aperture. The remaining part of the tip is the Al cladding. We assume that an incident electromagnetic field locally illuminates the core region of the tip. To obtain the self-consistent response of the tip/sample system to the incident field, we use the coupled, discrete dipole approach. We divide the tip and the sample into small subvolumes. The optical response of each subvolume is characterized by an isotropic dipole polarizability determined from the relative dielectric constant of the tip or sample material. The self-consistent local fields in the tip and the sample are determined using the photon Greens function. Once the local fields have been calculated, we calculate the transmitted light collected in the far-field region using the asymptotic electric fields radiated from the tip and the sample.

We also calculate the transmitted light scattered by Au nanoparticle using the BB field as the model for the illumination. The BB model can account for the aperture size but not for the finite thickness of the cladding. In the BB model, the tip field component along the direction of incident polarization is located primarily inside the

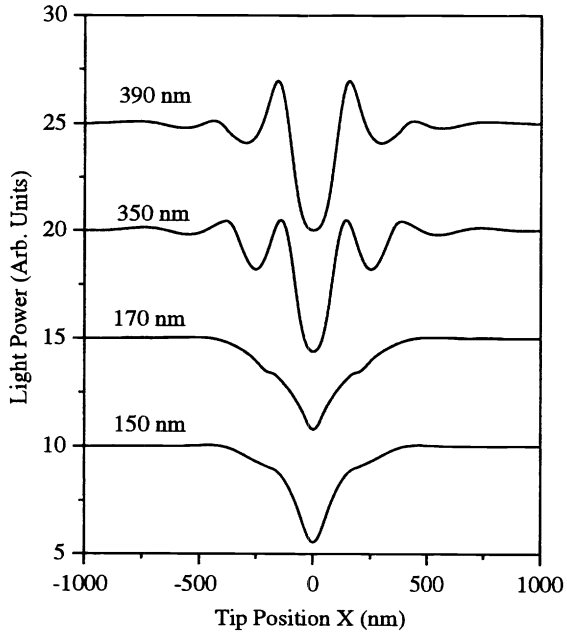

Figure 4. X scans for the NSOM images of a 100 nm×100 nm×60 nm (x, y, z) Au particle calculated in the disk model for different tip sizes. The tip core radius is 70 nm. The outer tip radii used in the calculations are indicated in the figure. The tip-sample separation in the z direction is 20 nm.

aperture and the component normal to the aperture is located near the aperture edge. The field distribution in the xy plane is also broader parallel to the polarization than perpendicular to the polarization. When a finite cladding is modeled, as with the disk model, the fields can be significantly different. First, the field distribution is broader perpendicular to the polarization than parallel to the polarization. This occurs because the distribution of the tip field component along the polarization is pushed farther from those tip sidewalls where that component is suppressed by the metallic depolarization. Furthermore, there is a substantial enhancement of the field beneath the cladding at the tip end when the cladding is thicker than $\lambda/2$. These differences between the tip fields for the BB and disk models lead to significant differences in the simulated images.

3.3. Simulations

Calculated line scans for the observed NSOM images show a strong dependence on tip aperture size and cladding width. The key features of images formed with both blunt and sharp tips are reproduced by our model when we use a thin disk to model the end of the tip. For images made with blunt tips the model predicts the triplet structure for scans along the direction of the incident-field polarization (we take these to be the x-scans, see Fig. 4) and the broader central minimum without side maxima for y-scans, see Fig. 5. We correctly predict the widths of the central minimum and the position of the side maxima. The additional side maxima in the x-scans arise because there is a strong enhancement in the fields just below the tip cladding along the polarization direction. When the cladding width is less than half a wavelength, as for sharp tips, this field enhancement is suppressed and the side maxima disappear. We predict prominent interference oscillations only for y-scans with sharp tips. Images calculated using the simple Bethe-Bouwkamp model for the tip fields, see Fig. 6, fail to reproduce these essential features. No side maxima are seen for this model because there is no enhancement of the field under the screen. Moreover, the Bethe-Bouwkamp model predicts that central minima are almost the same for x-scans and for y-scans in contrast to both the experiments and our disk model calculations.

From a comparison of the experimental and simulated images, it is clear that essential features in the images arise from the detailed structure of the tip field. Since the Au nanoparticle is smaller than the tip aperture and

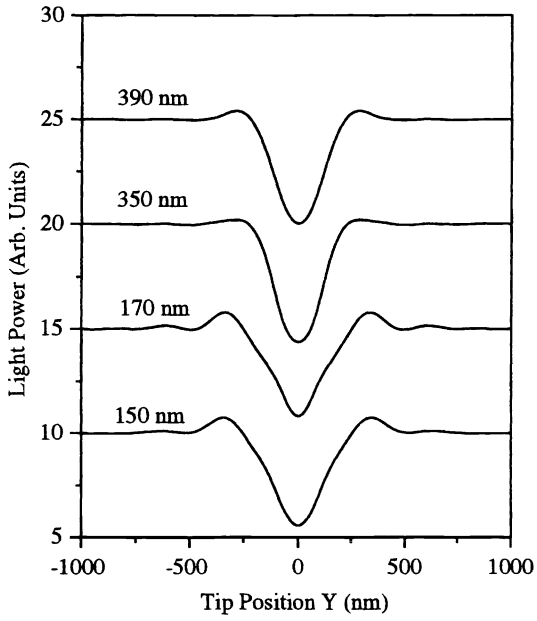

Figure 5. Y scans for the NSOM images of a 100 nm×100 nm×60 nm (x, y, z) Au particle calculated in the disk model for different tip sizes. The tip core radius is 70 nm. The outer tip radii used in the calculations are indicated in the figure. The tip-sample separation in the z direction is 20 nm.

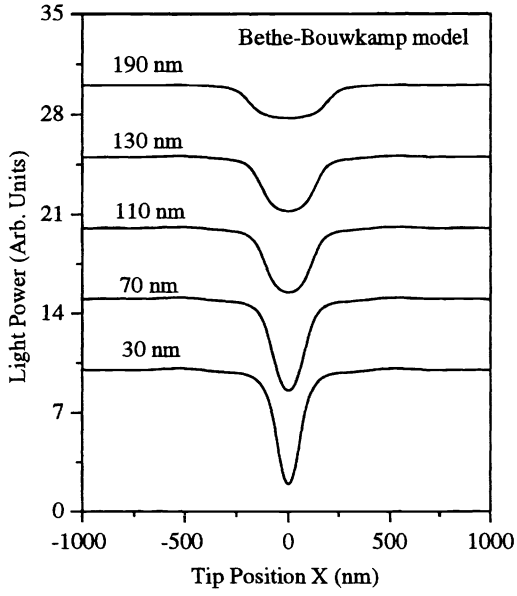

Figure 6. X scans for the NSOM images of a 100 nm×100 nm×60 nm (x, y, z) Au particle calculated in the Bethe-Bouwkamp model for different aperture sizes, i.e. 30, 70, 110, 130, and 190 nm. The tip-sample separation in the z direction is 20 nm.

the cladding thickness, the nanoparticle acts as a probe of the tip fields and is able to image and resolve different structures in the tip field. A simple model like the BB model cannot reproduce essential features in the tip field distribution that arise because the tip has a cladding with a finite thickness. Thus the BB model is a poor model to use to simulate images made when the sample acts, effectively, as a probe of the tip. More detailed models, such as the disk model, provide a better representation of the tip field and can reproduce the experimental images.

4. CONCLUSIONS

To fully exploit near-field optical microscopy, one must be able to interpret, analyze and understand NSOM images. Experiments with well characterized tips and simple samples are needed to produce basic NSOM images. Detailed modeling to simulate images and identify essential features in the image formation is required. We have presented two examples in which a comparison between the experimental images made of simple samples and the simulated images obtained from a detailed model has been made. We are able to identify the essential features in the image formation and provide a understanding for the structure in the images for each case because the models accounted for the entire process of image formation, including the illumination, scattering and collection. NSOM imaging of nanochannel glass arrays depends critically on the fields in the sample, how they couple to the tip field, and how they are scattered to and collected in the far field. NSOM imaging of Au nanoparticles depends critically on the detailed structure of the tip field. These two examples show that all parts of the image formation process must be included for a detailed understanding of NSOM images.

ACKNOWLEDGMENTS

This work is the result of extensive collaboration with E. L. Shirley, L. S. Goldner, E. B. McDaniel, J. W. P. Hsu, R. J. Tonucci, L. J. Richter and S. J. Strannick. Their efforts have been critical and are gratefully acknowledged.

REFERENCES

1. D. W. Pohl, "Scanning near-field optical microscopy (NSOM)," in *Advances in Optical and Electron Microscopy Vol. 12*, C. J. R. Sheppard and T. Mulvey, eds., pp. 243–312, Academic, London, 1991.
2. D. Courjon and C. Bainier, "Near field microscopy and near field optics," *Rep. Prog. Phys.* **57**, pp. 989–1028, 1994.
3. M. A. Paesler and P. Moyer, *Near Field Optics: Theory, Instrumentation, and Applications*, Wiley, New York, 1996.
4. C. Girard and A. Dereux, "Near-field optics theories," *Rep. Prog. Phys.* **59**, pp. 657–699, 1996.
5. E. B. McDaniel, J. W. P. Hsu, L. S. Goldner, R. J. Tonucci, E. L. Shirley, and G. W. Bryant, "Local characterization of transmission properties of a two-dimensional photonic crystal," *Phys. Rev. B* **55**, pp. 10878–10882, 1997.
6. R. J. Tonucci, B. L. Justus, A. J. Campillo, and C. E. Ford, "Nanochannel array glass," *Science* **258**, pp. 783–785, 1992.
7. J. D. Joannoupoulos, R. D. Meade, and J. N. Winn, *Photonic Crystals*, Princeton University Press, Princeton, 1995.
8. G. W. Bryant, E. L. Shirley, L. S. Goldner, E. B. McDaniel, J. W. P. Hsu, and R. J. Tonucci, "Theory of probing a photonic crystal with transmission near-field optical microscopy," *Phys. Rev. B* **58**, pp. 2131–2141, 1998.
9. H. A. Bethe, "Theory of diffraction by small holes," *Phys. Rev.* **66**, pp. 163–182, 1944.
10. C. J. Bouwkamp, "On Bethe's theory of diffraction by small holes," *Philips Res. Rep.* **5**, pp. 321–332, 1950.
11. C. J. Bouwkamp, "On the diffraction of electromagnetic waves by small circular disks and holes," *Philips Res. Rep.* **5**, pp. 401–422, 1950.
12. L. J. Richter, C. E. Jordan, R. R. Cavanagh, G. W. Bryant, A. Liu, and S. J. Strannick, "Influence of secondary tip shape on illuminaton mode NSOM images," *J. Opt. Soc. A* , submitted.
13. A. Liu, G. W. Bryant, L. J. Richter, and S. J. Strannick, "Model calculation of illumination-mode near-field optical microscopy images of Au nanoparticles," preprint.
14. S. J. Strannick, L. J. Richter, and R. R. Cavanagh, "High efficiency, dual collection mode near-field scanning optical microscope," *J. Vac. Sci. Technol B* **16**, pp. 1948–1952, 1998.